Oligothiophene-Naphthalimide Hybrids Synthetic Approaches

Subjects: Others

Contributor: Elena Gala Sánchez, Matías Jesús Alonso Navarro, Jose L. Segura

Different variables were tuned in a series of organic semiconductors synthesized in the group of José L. Segura, such as the planarity and the length of their π-conjugated backbones, the topology and energy levels of the frontier molecular orbitals (HOMO and LUMO) and their molecular dipole moments. Studies carried out in the group of Rocío Ponce-Ortiz show that the tuning of these properties can be connected with the microstructure properties observed by atomic force microscopy (AFM) and X-ray diffraction (XRD) in thin films as well as with the performances in organic field-effect transistors (OFETs).

Keywords: organic electronics ; oligothiophene–naphthalimide ; semiconductor ; frontier molecular orbitals ; ambipolarity ; thin films ; organic field-effect transistors ; degradation of contaminants

1. Introduction

π-Conjugated small molecules and polymers are extensively used in organic electronics because of their low-cost manufacturing, light weight, good processability and good ability to be deposited on flexible substrates [1][2] in comparison with conventional inorganic semiconductors.[3][4] In order to efficiently tune the charge transport abilities and electronic performances of π-conjugated materials in (opto)electronic devices, an in-depth understanding of their molecular structures, supramolecular organization and film morphology are required. Among the most extensively investigated electron accepting organic materials, naphthalenediimides (NDI) [5][6][7] and perylenediimides (PDI) [1][8] stand out because of their good electron-withdrawing abilities and their low-lying LUMO levels, which properly stabilize multiple negative charges. On the other hand, thiophene-based π-conjugated oligomers and polymers are efficient electron-donor systems with tunable HOMO levels, suitable to stabilize multiple positive charges.

For these reasons, donor-acceptor assemblies based on oligothiophene and naphthalimide moieties have received a great deal of attention in organic electronics.[1][4][9] In this framework, during the last decade, the group of José L. Segura has been active in the syntheses of oligothiophene–naphthalimide assemblies in which the donor and acceptor electroactive units are connected through rigid heterocycles. The connection of flat and rigid donor and acceptor moieties through rigid heterocyclic spacers is an efficient strategy to minimize skeletal distortions, allowing closer intermolecular π–π stacking and extended intramolecular π conjugation. Furthermore, through the suitable functionalization of these innovative organic semiconductors, they can be designed to exhibit a good film forming ability and low reorganization energies for both electron and hole transports.

Theferore, in this entry we summarize the contribution of the group of José L. Segura to the development of synthetic strategies toward several families of ambiopolar electronic materials based on oligothiophene and 1,8-naphthalimide units connected via different families of oligothiophene-naphthalimide assemblies (Figure 1).

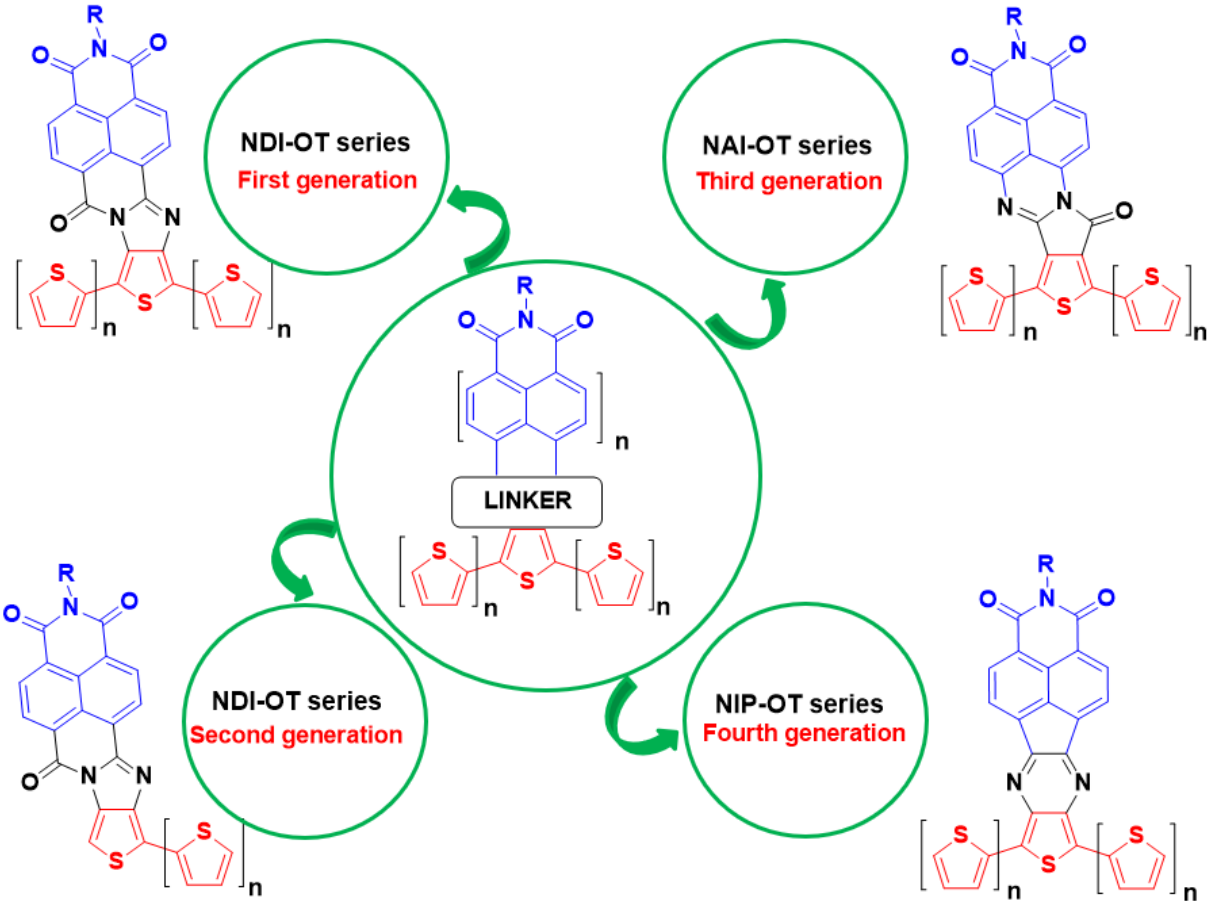

Figure 1. Oligothiophene-Naphthalimide Hybrids Connected through Rigid and Conjugated Linkers.

2. Amidine based Oligothiophene-Rylenimide Semiconductors

Our first approach to the desired hybrids connected through a rigid and conjugated linker involved the syntheses of thiophene-fused rylenimide derivatives via imidazole linkers. This first generation of organic semiconductors was obtained by condesation between suitable a diaminooligothiophene unit and the corresponding monoanhydride monoimide derviative (Scheme 1)

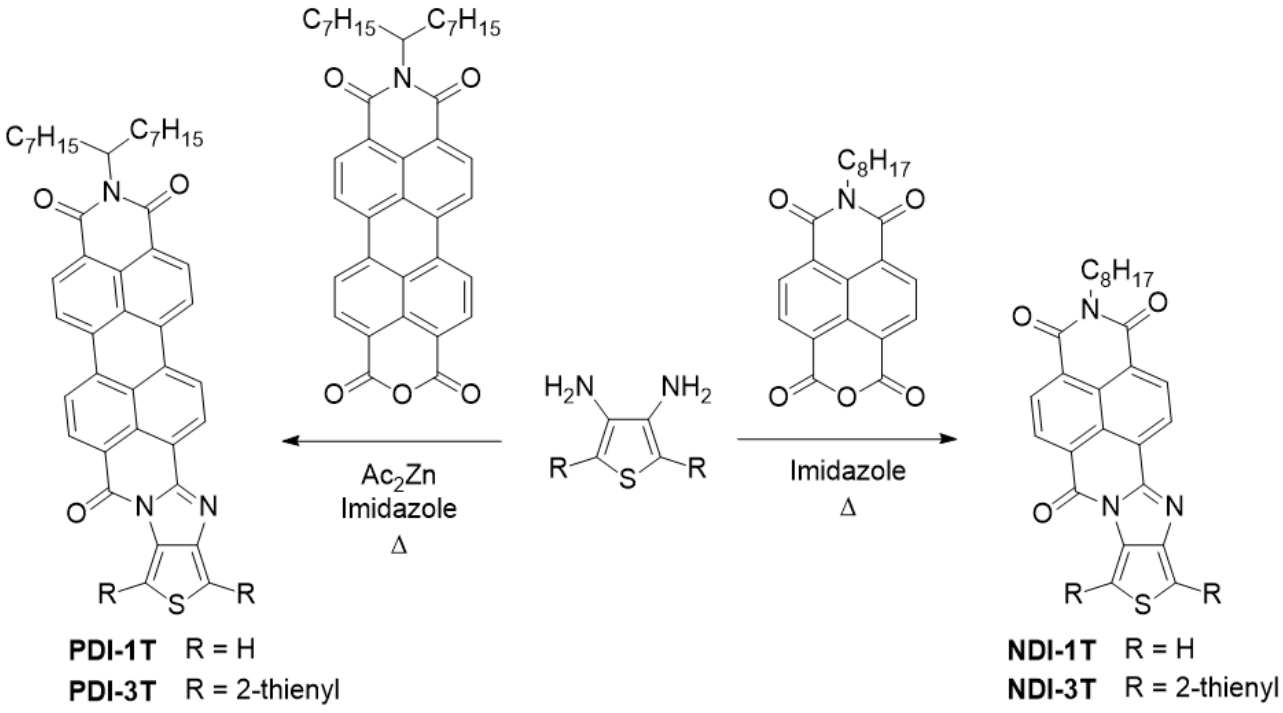

Scheme 1. Synthesis of NDI and PDI derivatives

Electrochemical characterization of these assemblies was carried out by using cyclic voltammetry measurements. Both reduction and oxidation processes were observed in all the naphthalene- and peryleneimide derivatives (Table 1). From these data, LUMO and HOMO energies could be estimated using standard approximations (Figure 2 and Table 1) [16,17], being -3.79/-5.83 eV for **NDI-1T** and -3.87/-5.55 eV for the **NDI-3T** analogue. A slight stabilization of the LUMO and a remarkable destabilization of the HOMO energy level around 0.3 eV, is observed when the oligothiophene fragment is extended. This electrochemical band gap reduction is consistent with the band gap compression observed in the UV-vis spectra. Further reduction of the electrochemical band gap can be achieved by extending the π-system of the rylenimide unit through replacement of the naphthalimide moiety by the larger perylenimide analogue. Thus, LUMO/ HOMO energies were estimated to be -3.88/-5.76 eV for **PDI-1T** and -3.89/-5.55 eV for **PDI-3T**. The extension of the oligothiophene moiety does not significantly alter the LUMO level while produces a destabilization of the HOMO level.

Table 1. Electrochemical potentials versus SCE in CH_2Cl_2 (referenced to Fc/Fc^+ couple) of **NDI-1T**, **NDI-3T**, **PDI-1T**, **PDI-3T** and **NDI-T-Ph-T** and Frontier Molecular Orbital Energy levels estimated from CV data.

Semiconductor	E_{red1}	E_{red2}	E_{ox1}	E_{ox2}	E_g^{CV}	LUMO[b]	HOMO[c]
NDI-1T	- 0.65	- 1.04	1.39 [a]		2.04	- 3.79	- 5.83
NDI-3T	- 0.57	- 0.93	1.11 [a]		1.68	- 3.87	- 5.55
PDI-1T	- 0.56	- 0.74	1.32 [a]		1.88	- 3.88	- 5.76
PDI-3T	- 0.55	- 0.71	1.06[a]		1.61	- 3.89	- 5.50

[a] Irreversible. [b] LUMO energy levels estimated vs vacuum level from E_{LUMO} = -4.44 eV - e E_{red1}. [c] Estimated from HOMO = LUMO – E_g^{CV}. E_g^{CV} = electrochemical gap.

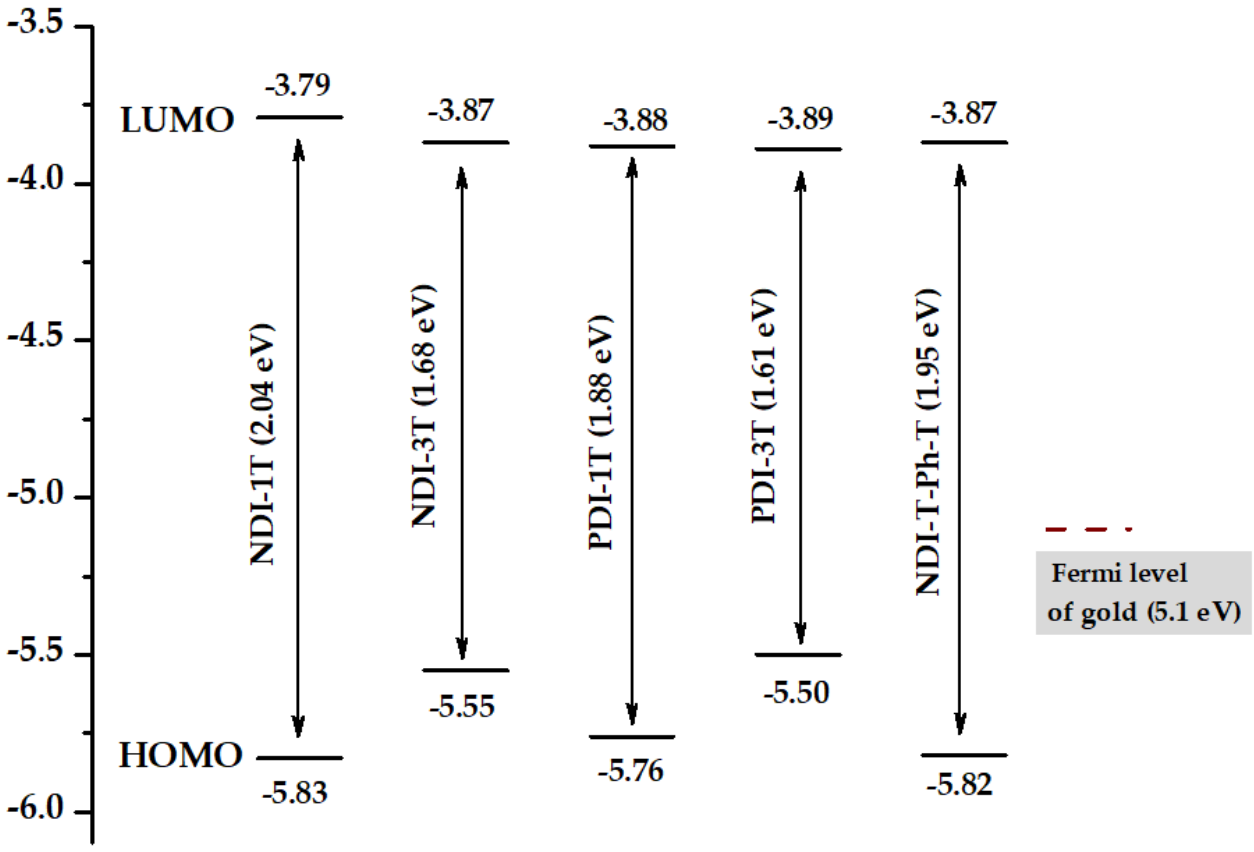

Figure 2. HOMO and LUMO energy levels for **NDI-3T, NDI-3T, PDI-1T, PDI-3T** and **NDI-T-Ph-T**

In order to evaluate the electrical performances of these first-generation of oligothiophene-rylenimide semiconductors, films were grown and applied to top-contact-bottom gate (TC/BG) field effect transistors in the group of Prof. Rocío Ponce-Ortiz at the Malaga University. The films were obtained either by vapor deposition or solution processed onto Si/SiO_2 substrates pre-treated with HDMS or OTS. The best degree of crystallinity was found for **NDI-1T** because of the formation of cofacial π-conjugated planes aligned to the Si/SiO_2 surface with a calculated tilt angle of 61,2°. In contrast, **NDI-3T** thin films resulted into an amorphous material probably due to the lack of planarity caused by sulfur-oxygen repulsion interaction which forces the disruption of the oligothiophene planarity. Although they are less crystalline than **NDI-1T**, the presence of sharp Bragg reflections in the X-ray diffractograms of **PDI-1T** and **PDI-3T** evidenced the existence of a certain degree of crystallinity in the perylene derivatives.

TC/BG field-effect transistors properties were evaluated in terms of charge carrier mobility (μ), current on-off ratio (I_{ON}/I_{OFF}) and threshold voltage (V_T) (Table 2). The best charge transport characteristics were found for **NDI-1T** when vapor-deposited films were grown at 110 °C on Si/SiO_2 surfaces treated with HMDS, with electron mobilities reaching values of 0.35 $cm^2V^{-1}s^{-1}$. These good results regarding **NDI-1T** could be explained in terms of high crystallinity, good molecular packing in well-connected grains as observed in XRD and AFM analyses. The smaller grain sizes and lower crystallinity observed for **PDI-1T** with a more extended π-conjugated system accounts for the slightly lower electron mobility of 0.1 $cm^2V^{-1}s^{-1}$ measured for this system. Regarding naphthalimide-based assemblies, the introduction of the phenylene moiety in **NDI-T-Ph-T** enhanced the crystallinity and the presence of well-defined and well-connected smaller grains, allowing mobilities of around 0.1 $cm^2V^{-1}s^{-1}$ for electron transport. Finally, the introduction of catenated thiophene units in both **NDI-3T** and **PDI-3T** decreases their performances in the devices in around two orders of magnitude in agreement with the analyses of AFM images and XRD patterns. In contrast with the analogue with one thiophene unit (**NDI-1T**), the introduction of additional thiophene moieties in **NDI-3T** produce a twist in the oligothiophene backbone thus hindering an efficient packing and therefore causing a decrease in the crystallinity of the films. As a result, electron mobilities of only 10^{-4} $cm^2V^{-1}s^{-1}$ can be measured for these assemblies. In comparison with the naphthalimide containing assembly **NDI-3T**, films made from the perylenimide containing analogue, **PDI-3T**, are more crystalline, having larger grains that allow better charge carrier mobilities of up to 10^{-3} $cm^2V^{-1}s^{-1}$. Solution processed OTFT transistors were also fabricated, and their morphologies and crystal structures were evaluated. The results obtained for these semiconductors were in good agreement with the new morphologies obtained for each one and, in the case of **PDI-3T**, an electrical enhancement was found in comparison with the vapor-deposited thin-film transistors.[10]

Table 2. OTFT Electrical data for Vapour-Deposited films of **NDI-1T**, **NDI-3T**, **PDI-1T**, **PDI-3T** and **NDI-T-Ph-T** measured under vacuum on Si/SiO_2 substrates.[a]

Semiconductor	S [b]	T_d (°C) [c]	μ_e	V_T	I_{ON}/I_{OFF}
NDI-1T	H	110	0.35	28	10^6
	O	110	0.10	28	10^5
	S	110	$1.2x10^{-2}$	55	10^2
NDI-3T	H	110	$2x10^{-4}$	10	10^2
	H	25	$3.5x10^{-4}$	45	10^3
PDI-1T	H	110	0.15	27	10^7
PDI-3T	H	110	$1.3x10^{-3}$	45	10^4
	O	110	$3.5x10^{-2}$	45	10^5
NDI-T-Ph-T	H	25	$7.4x10^{-2}$	45	10^6
	O	25	0.10	58	10^5

[a] Electron carrier mobility (μ) is given in $cm^2V^{-1}s^{-1}$ and threshold voltages (V_T) in V. [b] Device parameters reported are for films grown on untreated Si/SiO_2 substrates (S), hexamethyldisilazane vapor-treated Si/SiO_2 substrates (H) or octadecyltrichlorosilane-treated Si/SiO_2 substrates (O). [c] Deposition temperature

Motivated by the above results,[10] a novel family of naphthalimide-oligothiophene assemblies[11] (second-generation **NDI-nT**) was designed with the aim to avoid the above described skeletal distortion (Figure 3).

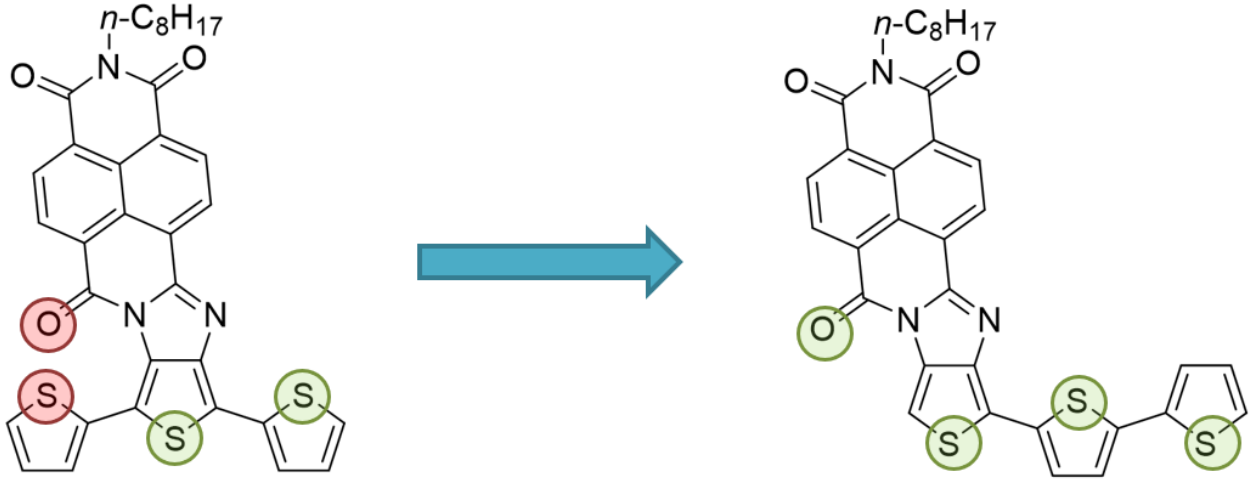

Figure 3. Schematic representation of oxygen-sulfur repulsive interaction (highlighted in red) in the first generation of NDI-oligothiophene derivatives and how it is suppressed in the second generation.

In order to obtain this second generation of oligothiophene-naphthalimide assemblies, a linear synthetic approach was followed (Scheme 2) instead of the convergent one used previously.[10][12][13] Thus, a monobrominated thiophene-naphthalimide derivative (**NDI-1T-Br**, Scheme 2) was used as starting material. Stille cross-coupling reactions between **NDI-1T-Br** and the corresponding monostannane derivatives were carried out in order to obtain the target molecules **NDI-2T**, **NDI-3Tp** and **NDI-4T** in good yields.[11] As depicted in Scheme 2, the steric repulsion between the oxygen and sulfur heteroatoms is absent in these new organic semiconductors thus preventing the skeletal distortions. Additionally, **NDI-5T** (Scheme 2) was synthesized for comparison purposes given that it combines a fragment with the extended π conjugated structure of **NDI-3Tp** and also a fragment with the steric hindrance of **NDI-3T**. **NDI-5T** could be obtained by Suzuki cross-coupling reaction between **NDI-1T-2Br** and the 2,2′−Bithiophene-5-boronic acid pinacol ester.

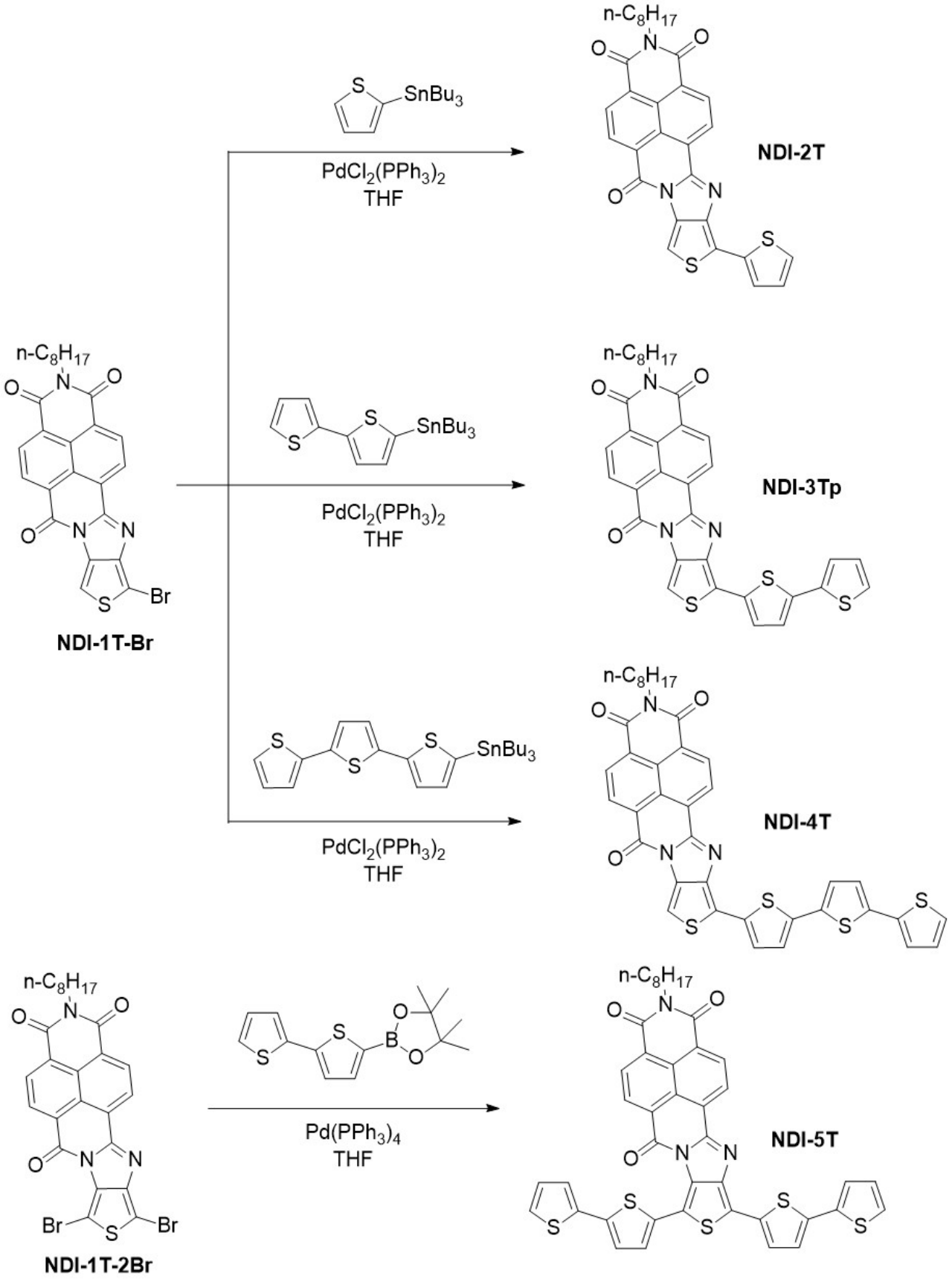

Scheme 2. Syntheses of **NDI-nT** materials.

The HOMO levels of **NDI-4T** and **NDI-5T** approaches the Fermi level of Au thus improving the hole injection in electronic devices.

It is also worth noting that the band gap of the planar **NDI-3Tp** is 0.1 eV smaller than that of the **NDI-3T** analogue with a distorted structure (Figure 4). This energy readjustment, in conjunction with other morphological and electronic factors, is probably the origin of the ambipolar behavior shown by **NDI-3Tp**.

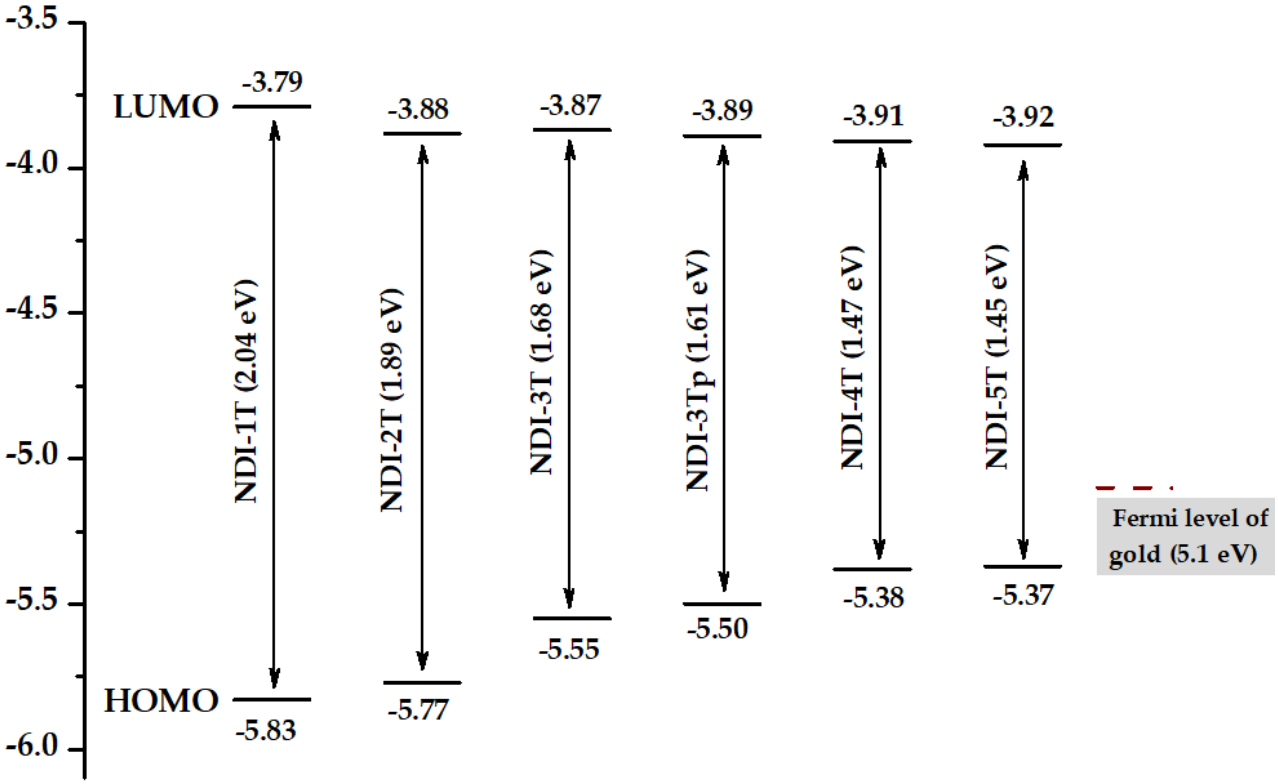

Figure 4. HOMO/LUMO energy levels derived from the electrochemical measurements. Energy gaps are shown in brackets.

Thin films of these **NDI-nT** semiconducting materials were processed from solutions or obtained by sublimation. X-ray analyses of the thin films show that crystallinity is much more pronounced in those films obtained by sublimation. The most remarkable characteristics of the FET performances of these semiconductors were investigated in TC/BG OFETs (Table 3). The shortest derivative, **NDI-2T**, only shows electron mobilities up to 2.6×10^{-2} $cm^2V^{-1}s^{-1}$. The fact that **NDI-2T** only exhibit *n*-type mobility values is consistent with the similarity of its HOMO energy level and that of **NDI-1T**. In contrast, ambipolarity was found for **NDI-3Tp** and **NDI-4T**. This ambipolar behavior could be related to: 1) the lack of skeletal distortions that allow close π-π stacking interactions and lower reorganization energies and 2) the presence of longer conjugated oligothiophene moieties with increased π conjugation lengths that allow a destabilization of the HOMO energy levels which approach the Fermi level of Au. Interestingly, FETs fabricated using **NDI-5T** exhibit ambipolar transport behavior with balanced electron and hole transport mobilities of approximately 10^{-5} $cm^2V^{-1}s^{-1}$. The study demonstrates that the absence of ambipolarity is mainly due to the disruption in the π conjugation while a decrease in the carrier mobility is induced by the skeletal distortions. Furthermore, there is a good correlation between the charge transport properties, the film microstructures and the ordered packing of non-distorted structures.

Table 3. OFET Electrical data for Vapour-Deposited films of **NDI-2T**, **NDI-3Tp**, **NDI-4T** and **NDI-5T** measured under vacuum on Si/SiO_2 substrates. Average field-effect mobilities are shown.[a]

Semiconductor	S [b]	T_d (°C) [c]	μ_e	V_T	I_{ON}/I_{OFF}	μ_h	V_T	I_{ON}/I_{OFF}
NDI-2T	H	110	1.41×10^{-2}	31	10^5			
	H	25	2.11×10^{-3}	50	10^5			
NDI-3Tp	H	25	1.27×10^{-3}	34	2×10^2			
	O	25	1.83×10^{-3}	42	3×10^3	1.67×10^{-4}	- 62	$4 \cdot 10^2$
NDI-4T	H	110	7.53×10^{-3}	41	10^2	1.13×10^{-3}	- 51	10
	H	25	6.37×10^{-5}	28	3×10^2	4.79×10^{-5}	- 59	10^2
NDI-5T	H	110	3.21×10^{-6}	54	10^2			

[a] Electron carrier mobility (μ) is given in $cm^2V^{-1}s^{-1}$ and threshold voltages (V_T) in V. [b] Device parameters reported are for films grown on hexamethyldisilazane vapor-treated Si/SiO_2 substrates (H) or octadecyltrichlorosilane-treated Si/SiO_2 substrates (O). [c] Deposition temperature.

3. Inverted Amidine-Based Oligothiophene–Naphthalimide Semiconductors

The lessons learned from the first series of oligothiophene–naphthalimide assemblies allowed us to conclude that ambipolar semiconductors with these kinds of systems can be obtained by (i) connecting the donor and acceptor moieties through conjugated rigid linkers, (ii) avoiding steric hindrance and skeletal distortions and (iii) extending the effective π-conjugated length of the oligothiophene moiety.

In the search for new low-bandgap materials in which facile hole and electron injection are possible from a single type of electrode, we designed another new family of oligothiophene–naphthalimide assemblies, NAI derivatives (Figure 5) that involves the inversion of the amidine linkage connections between the oligothiophenes and the naphthalimide in order to prevent steric interactions (Figure 5).[14]

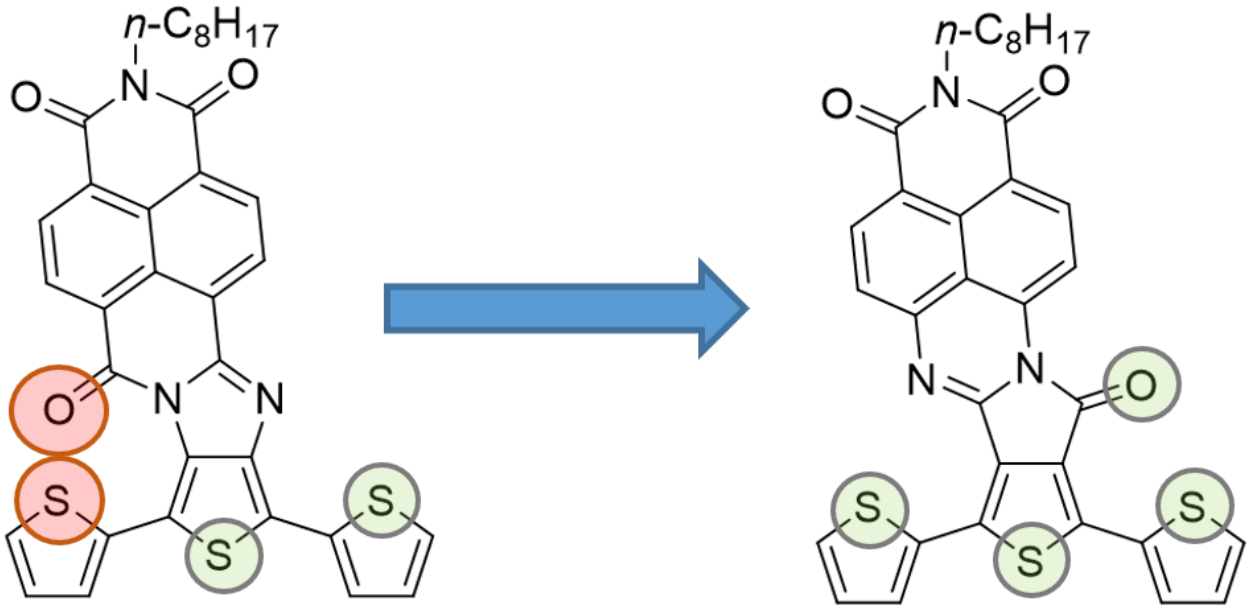

Figure 5. Illustration of the oxygen–sulfur interaction in **NDI-3T** and **NAI-3T** derivatives.

As it is depicted in scheme 3, for the syntheses of the NAI derivatives, naphthalimide moieties endowed with amino functionalities and a thiophene derivative endowed with anhydride functionality were used as starting materials. Through a condensation reaction between the mentioned monomers, the dibrominated **NAI-1T-2Br** derivative can be obtained. Further reaction of **NAI-1T-2Br** by Stille cross-coupling reactions with the corresponding stannylated thiophene or bithiophene yield the target molecules **NAI-3T** and **NAI-5T**. In terms of the molecular structure, the inversion in the orientation of the carbonyl group in the imidazole unit provides more planar semiconductors, in which the O···S repulsive interaction is deliberately avoided in contrast with that observed in the first generation of oligothiophene–naphthalimide assemblies with noninverted amidine linkers.[10][11]

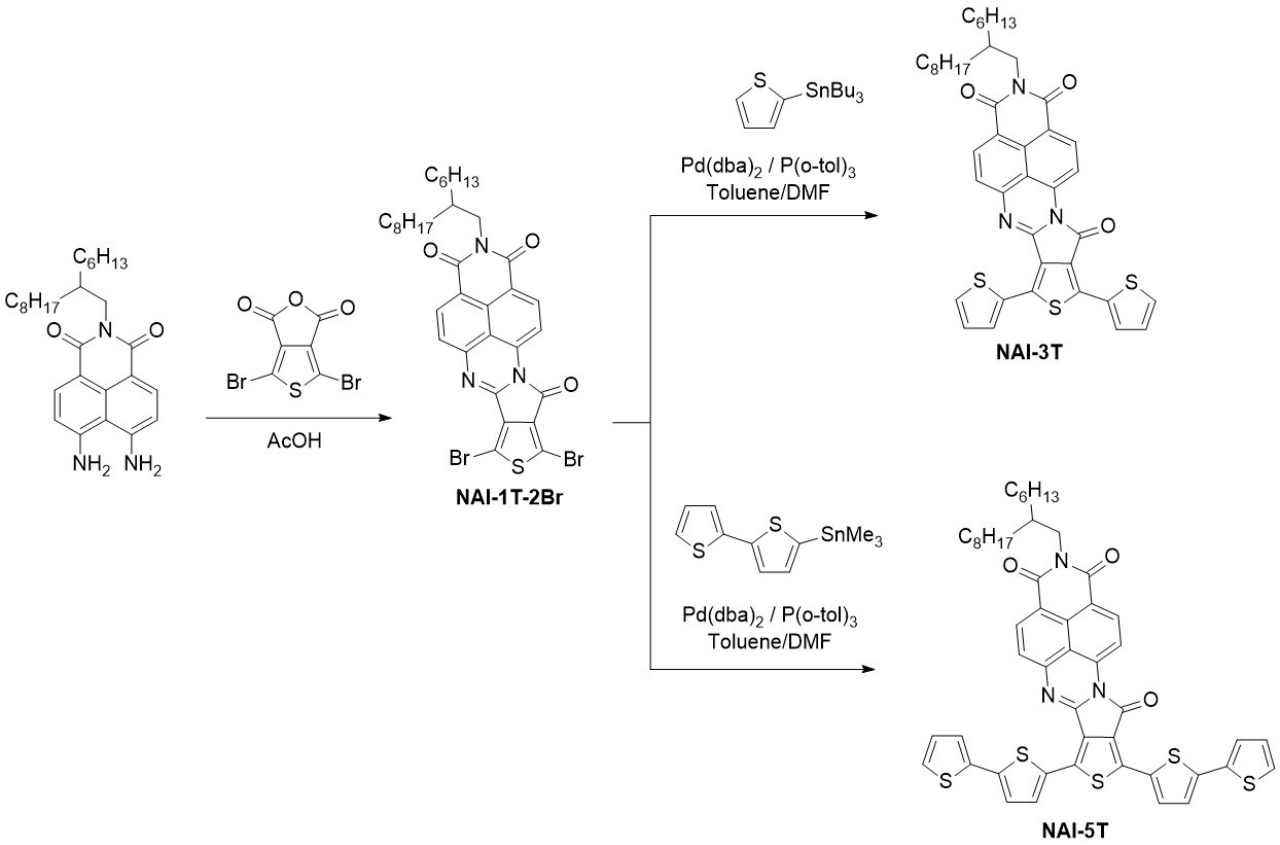

Scheme 3. Syntheses of the fourth generation of oligothiophene–naphthalimide assemblies.

Cyclic voltammetry measurements for both **NAI-3T** and **NAI-5T** present oxidation and reduction processes. From these values, the HOMO and LUMO energy levels could be estimated (Figure 6). The LUMO energy levels estimated for the NAI derivatives are significantly destabilized in comparison with those of the NDI analogues, while the HOMO energy levels of both **NAI-3T** and **NAI-5T** are more stabilized than those corresponding to their NDI counterparts.[10][11][15]

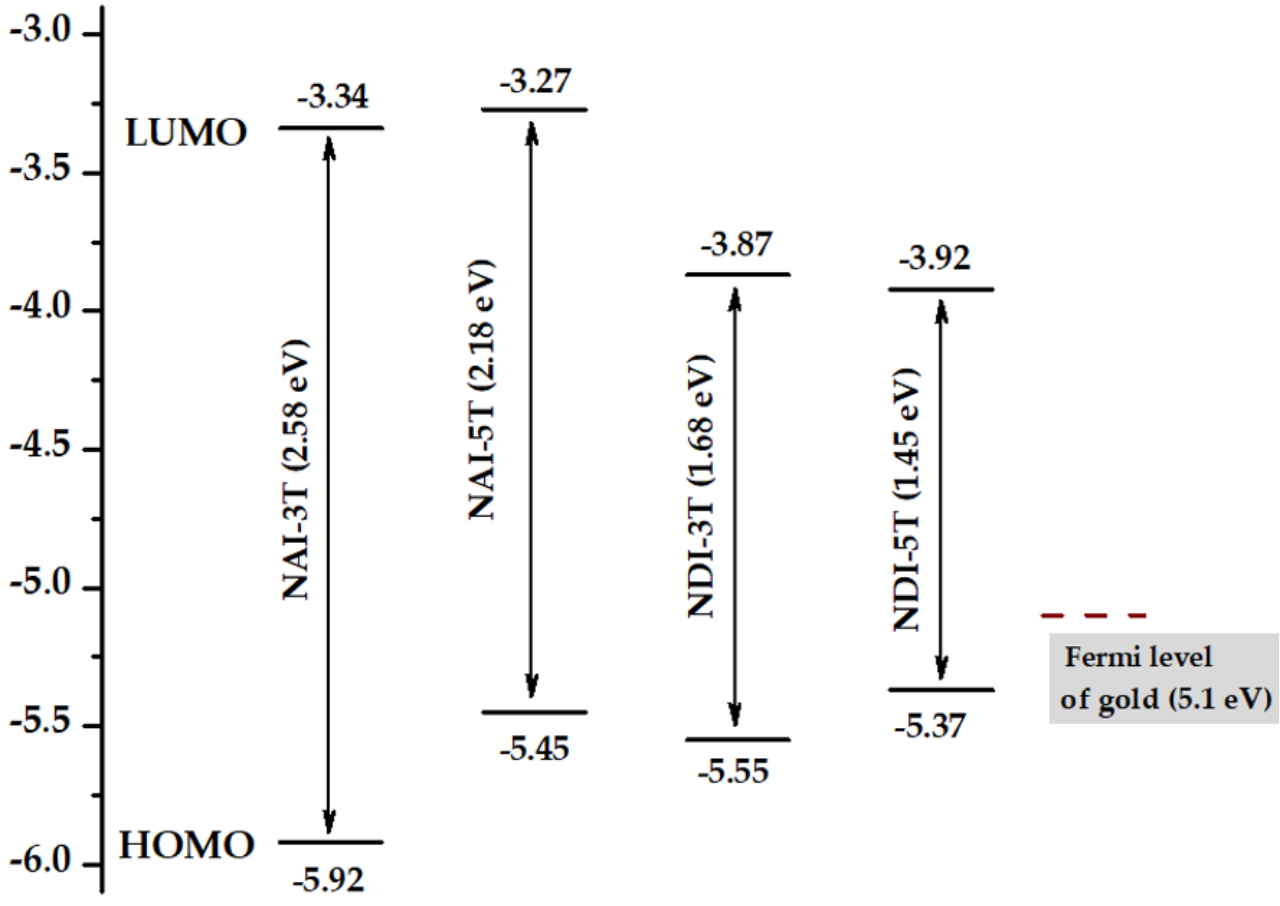

Figure 6. HOMO/LUMO energy levels for oligothiophene–naphthalimide assemblies based on NDI and NAI.

Finally, in order to evaluate the electrical properties of these new semiconductors, TC/BG field-effect transistors were fabricated by vapor deposition. The OFET performance obtained for the vapor-deposited films is summed up in Table 4. In this semiconductor series, p-type and ambipolar transport properties were found for **NAI-5T** and **NAI-3T**, respectively. In the shorter member of the series, the electron mobilities are similar to that of the NDI analogues, around 1.9 × 10^{-4} cm^2 V^{-1} s^{-1}, with interesting balanced values for hole mobilities of 2.0 × 10^{-4} cm^2 V^{-1} s^{-1} at 25 and 110 °C. Although the outputs for **NAI-5T** show clear ambipolarity, only hole-charge transport values of 5.75 × 10^{-5} cm^2 V^{-1} s^{-1} were ultimately measured. The better hole mobility values obtained for **NAI-5T** in comparison with the parent **NDI-5T** could be related to the HOMO delocalization over the whole molecule, which allows better orbital overlapping between molecules.

Table 4. OFET electrical data for vapor-deposited films of **NAI-3T** and **NAI-5T** measured under vacuum on Si/SiO_2 substrates. Average field-effect mobilities are shown [a].

Semiconductor	S [b]	T_d (°C) [c]	μ_e	V_T	I_{ON}/I_{OFF}	μ_h	V_T	I_{ON}/I_{OFF}
NAI-3T	O	110	$1.15x10^{-4}$	42	10	$2x10^{-4}$	- 40	$5x10^2$
	O	25	$1.95x10^{-3}$	39	20	$2x10^{-3}$	- 46	$3x10^2$
NAI-5T	H					$5.75x10^{-5}$	- 41	10^2

[a] Electron carrier mobility (μ) is given in $cm^2V^{-1}s^{-1}$ and threshold voltages (V_T) in V. [b] Device parameters reported are for films grown on hexamethyldisilazane vapor-treated Si/SiO_2 substrates (H) or octadecyltrichlorosilane-treated Si/SiO_2 substrates (O). [c] Deposition temperature.

4. Pyrazine-Based Oligothiophene–Rylenimide Semiconductors

As it was previously shown, avoiding steric hindrance and skeletal distortions in naphthalimide-oligothiophene assemblies plays a crucial role in the search of ambipolarity. For that reason, we designed a fifth generation of naphthalimide-oligothiophene assemblies in which flat and rigid pyrazine units are used as conjugated linkers (Figure 7).

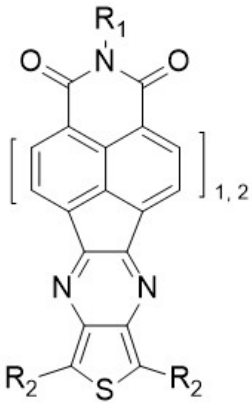

Figure 7. General structure of the fifth generation of oligothiophene-naphthalimide assemblies

The pyrazine-based materials can be obtained by condensation reactions between naphthalene- (**NID**) or peryleneimides (**PID**) endowed with 1,2-diketone functionalities, and the corresponding diaminothiophene derivatives (Scheme 4).[16][17]

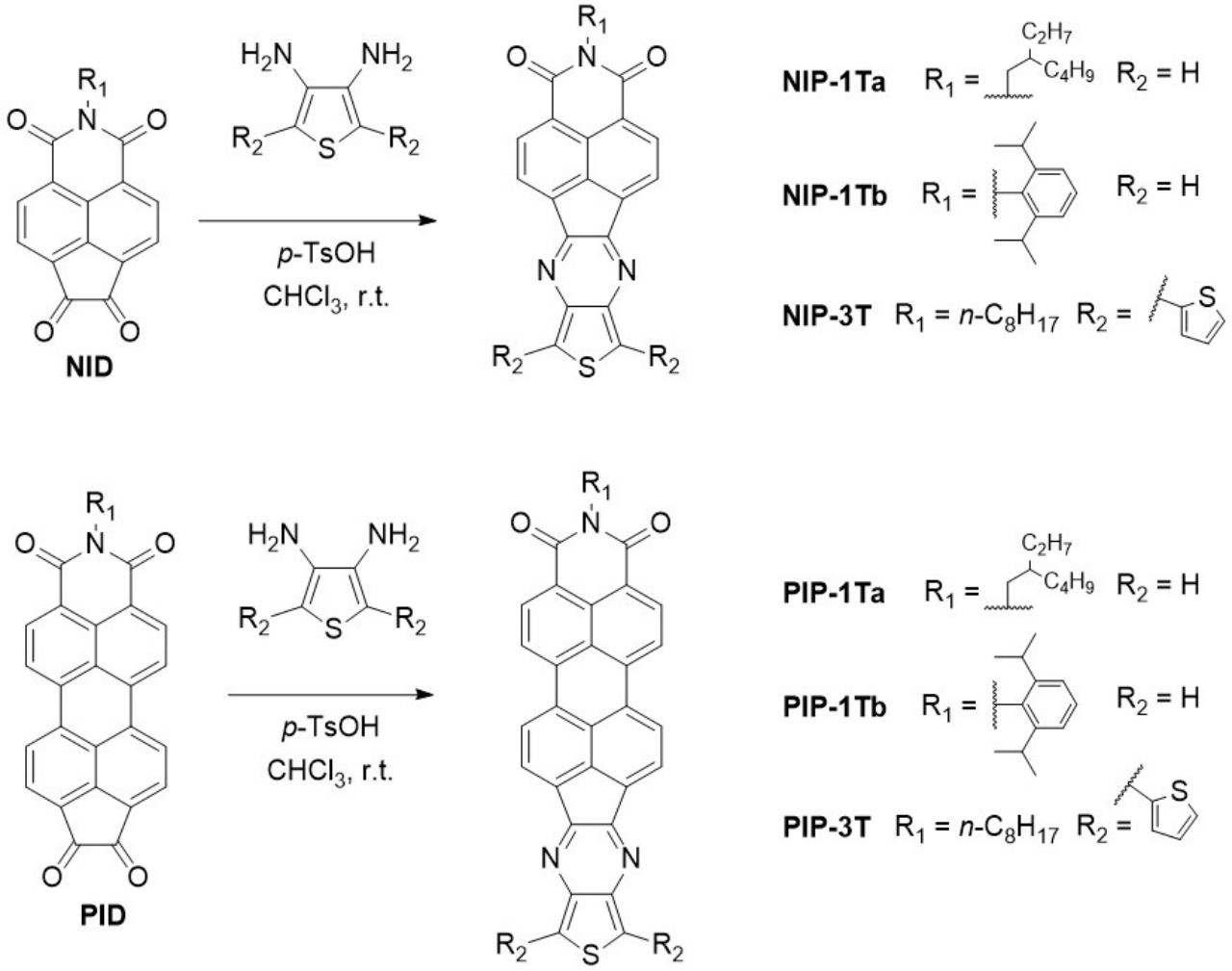

Scheme 4: Syntheses oligothiophene-naphthalimide (**NIP**) and perylenimide (**PIP**) assemblies with pyrazine linkers.

In order to study the electrochemical properties of these planar pyrazine-based assemblies, cyclic voltammetry experiments were carried out, and from the obtained electrochemical values, frontier molecular orbital energies could be estimated. As we previously described, oligothiophene chain catenation had an important effect over the HOMO energy, showing destabilized values as the oligothiophene is growing, whereas LUMO energies were barely altered.[11][15] Lowest unoccupied molecular orbital energy levels depend on the extension of the rylenimide units. Thus, the estimated LUMO values for **NIP-1T** and **PIP-1T** are -3.40 eV and -3.49 eV respectively. Regarding to the oligothiophene counterpart, an increment in the number of the thiophenes has negligible effect in the LUMO level, while this chemical modification affects clearly the HOMO energy levels, and therefore the optical band gap. The HOMO energy level estimated for **PIP-1T** (-5.34 eV) is significantly estabilized in comparison to that estimated for **PIP-3T** (-4.75 eV). The destabilization of the HOMO observed for **PIP-3T** is in good agreement with the extension of the thiophene backbone and with the absorption spectra. Therefore, in these pyrazine-based semiconductors, tuning the HOMO-LUMO bandgap can be achieved by two approximations: (i) by extending the rylenimide core without modifying the donor moiety and (ii) through the increment in the length of oligothiophene backbone. Comparison between the HOMO and LUMO energy levels of the NIP and PIP semiconductors and those of the NDI and PDI analogues reveals that the replacement of the imidazole linker by a rigid pyrazine heterocycle is reflected into more destabilized HOMO and LUMO orbitals, as well as in the enlargement of the band gap (Table 5).[11][17]

Table 5. Electrochemical potentials versus SCE in CH_2Cl_2 (referenced to Fc/Fc^+ couple) of **NIP-1T**, **NIP-3Ta**, **PIP-1T** and **PIP-3T** and Frontier Molecular Orbital Energies estimated from CV data.

Semiconductor	E_{red1}	E_{red2}	E_{ox1}	E_{ox2}	E_g^{CV}	E_g^{opt}	LUMO [b]	HOMO
NIP-1Ta	- 0.86	- 1.30	1.78 [a]		2.64	2.51	- 3.58	- 6.22 [c]
NIP-1Tb	- 0.95	- 1.33				2.51	- 3.49	- 6.00 [d]
NIP-3Ta	- 0.83	- 0.93	0.99 [a]	1.75 [a]	1.68		- 3.61	- 5.43 [c]
PIP-1Ta	- 0.72	- 0.99				2.01	- 3.72	- 5.73 [d]
PIP-1Tb	- 1.04	- 1.28				1.94	- 3.40	- 5.34 [d]
PIP-3T	- 1.11 [a]	- 1.41				1.43	- 3.33	- 4.76 [d]

[a] Irreversible. [b] LUMO energy level estimated vs vacuum level from E_{LUMO} = -4.44 eV - e E_{red1}. [c] Estimated from HOMO = LUMO – E_g^{CV}. E_g^{CV} = electrochemical gap. [d] Estimated from HOMO = LUMO – E_g^{opt}. E_g^{opt} = optical gap.

As a common evaluation of the electrical properties for these pyrazine-based oligothiophene-rylenimide derivatives, the fabrication of TC/BG thin-film organic field-effect transistors was accomplished. Concerning with the charge transport ability of these thienopyrazine derivatives, all of them showed *n*-type mobilities, with a best electron mobility value of $2.87 \cdot 10^{-4}$ $cm^2V^{-1}s^{-1}$ for **NIP-1T** when it was deposited at 50 °C on HMDS-treated dielectric (Table 6). **NIP-3T** is the only thienopyrazine derivative that show ambipolar behavior, with good balanced values for both hole and electron charge carriers. This effect is related with the high planar structure and low internal reorganization energies, enabling both electron and hole transport processes. The same behavior could be expected for **PIP-3T**, but only discrete n-type mobility was observed (1.2×10^{-4} $cm^2V^{-1}s^{-1}$). This result could be explained in terms of the formation of antiparallel π-π stackings among the molecules when they were vapor-deposited over the dielectric, restricting the formation of the D and A domains necessary for the hole and electron transporting. This aggregation behavior is in good agreement with the predicted computational study for dimeric species.[17]

Table 6. OFET Electrical data for Vapour-Deposited films of **NIP-1Ta**, **NIP-3Ta**, **PIP-1T** and **PIP-3T** measured under vacuum on hexamethyldisilazane vapor-treated Si/SiO_2 substrates. Average field-effect mobilities are shown.[a]

Semiconductor	S [b]	T_d (°C) [c]	μ_e	V_T	I_{ON}/I_{OFF}	μ_h	V_T	I_{ON}/I_{OFF}
NIP-1Ta	H	50	2.9×10^{-4}	47	3×10^4			
	H	25	1.3×10^{-5}	49	3×10^3			
NIP-3Ta	H	90	4.3×10^{-5}	47	4×10^4	4.10×10^{-5}	- 47	3×10^3
	H	25	1.0×10^{-4}	71	7×10^2	1.38×10^{-5}	- 65	5×10^2
PIP-1Ta	H	150	1.1×10^{-4}	33				
	O	150	1.5×10^{-4}	36				
	H	110	5.8×10^{-5}	31				
PIP-1Tb	O	110	1.2×10^{-4}	25				
PIP-3T [d]	O	130	1.2×10^{-4}	8				

[a] Electron carrier mobility (μ) is given in $cm^2V^{-1}s^{-1}$ and threshold voltages (V_T) in V. [b] Device parameters reported are for films grown on hexamethyldisilazane vapor-treated Si/SiO_2 substrates (H) or octadecyltrichlorosilane-treated Si/SiO_2 substrates (O). [c] Deposition temperature. [d] Solution processed film.

To further explore the possibility of tuning the performance of this type of material in (opto)electronic devices, we designed a family of oligothiophene–naphthalimide assemblies based on pyrazine linkers in which end-capped units were introduced in order to promote good packing in the molecule while the HOMO/LUMO energy levels are still suitable for semiconducting applications.[18]

These new thienopyrazine-based semiconductors are endowed with different substituents in order to promote molecular ordering, better processability and tuning of the frontier molecular orbitals. These oligothiophene–naphthalimide assemblies can be divided into different groups depending on the nature of the end-capped units introduced: (i) substituents that promote intermolecular interactions and (ii) different electron acceptors in order to modulate the HOMO/LUMO energy levels. Thus, there are three end-capped derivatives functionalized with pyrene, triisopropilsilyl and diphenylamine with a donor-acceptor-donor (**D-A-D**) structure (Scheme 5). On the other hand, the introduction of electron acceptor substituents via Knoevenagel-like reactions led to obtaining **A2-D-A1-D-A2** semiconductors endowed with rhodanine and dicyanovinylene end groups (Scheme 6).

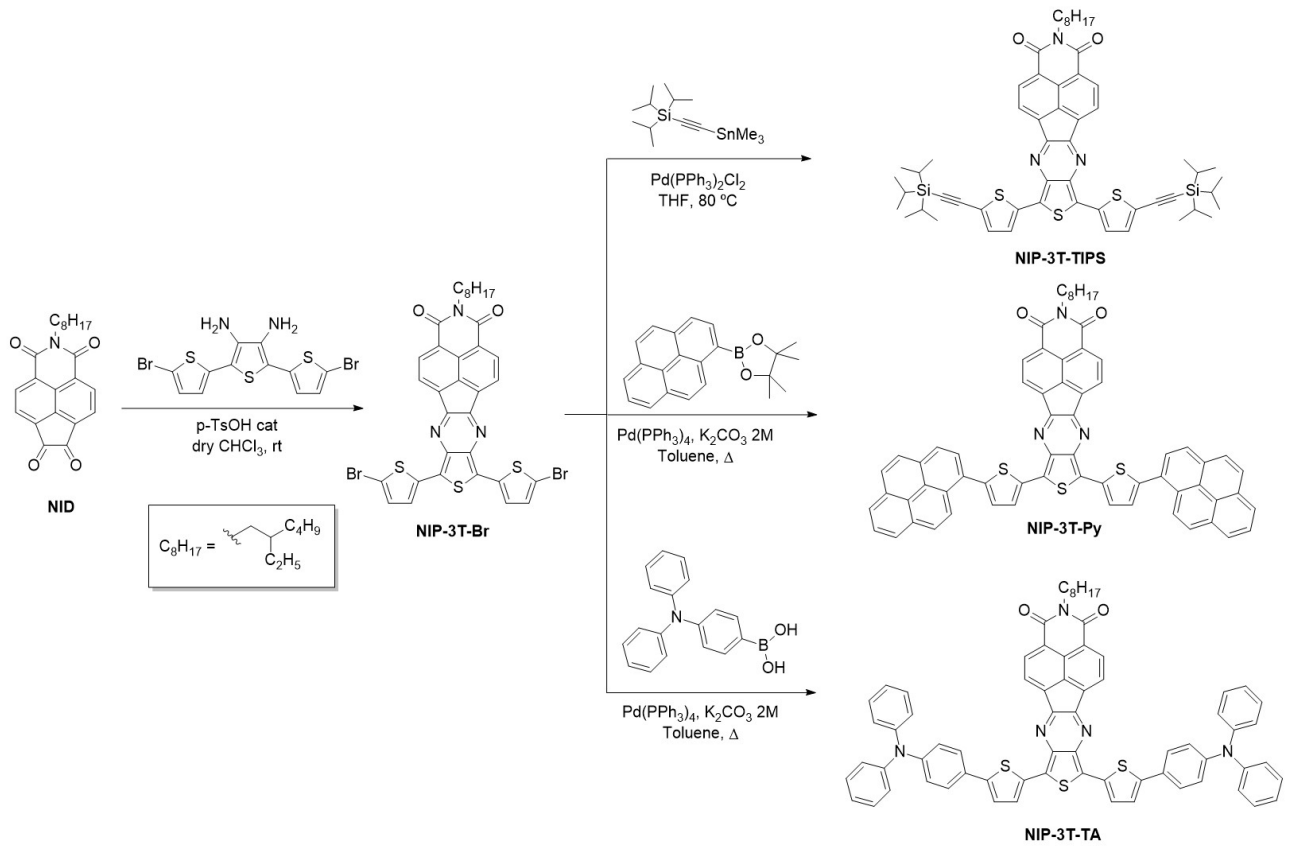

Scheme 5. Syntheses of **D-A-D** oligothiophene–naphthalimide assemblies.

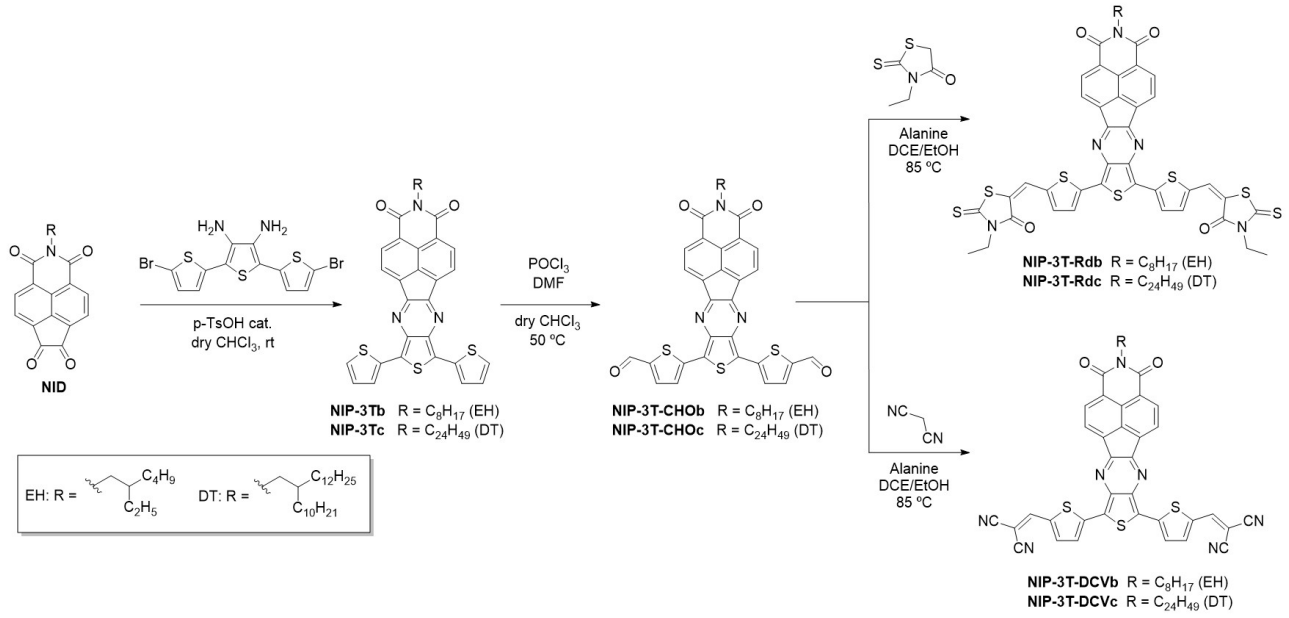

Scheme 6. Syntheses of **A2-D-A1-D-A2** oligothiophene–naphthalimide assemblies.

The electrical characterization of these new semiconductors was carried out in organic field-effect transistors with TC/BG architectures. The thin films deposited by vapor deposition were also characterized by XRD and AFM techniques. As previously shown, **NIP-3Tb** has ambipolar characteristics, with balanced holes and electron mobility values of 4×10^{-5} cm^2 V^{-1} s^{-1}. The introduction of lateral substituents modifies the polarity in the charge transport properties, as it was shown for **NIP-3T-TIPS**, in which only *p*-type characteristics were found. On the other hand, when pyrene moieties are introduced laterally in the **NIP-3T-Py** derivative, electron mobilities of 10^{-2} cm^2 V^{-1} s^{-1} were found, the best of all these semiconductors (Table 7). In contrast, when electron-withdrawing groups are introduced, only n-type mobilities were observed, except in the case of **NIP-3T-Rdb** in which ambipolarity is observed (Table 7). The different behavior observed for the end-capped oligothiophene–naphthalimide semiconductors can be also related to the limited crystallinity observed in XRD and AFM images. It is worth pointing out that, given the suitable HOMO and LUMO energy levels, as well as good processability and full absorption range even in the NIR spectra of the oligothiophene–naphthalimide assemblies endowed with electron-acceptor units, they have also recently received some attention as nonfullerene acceptors in OSCs.[18]

Table 7. OFET electrical data for vapor-deposited films of **NIP-3Tb**, **NIP-3T-DCVb**, **NIP-3T-Rdb**, **NIP-3T-Py** and **NIP-3T-TIPS** measured under vacuum on vapor-treated Si/SiO_2 substrates. Average field-effect mobilities are shown [a].

Semiconductor	S [b]	T_d (°C) [c]	μ_e	V_T	I_{ON}/I_{OFF}	μ_h	V_T	I_{ON}/I_{OFF}
NIP-3Tb	H	90	4×10^{-5}	47	7×10^{2}	4×10^{-5}	−47	3×10^{3}
NIP-3T-DCVb	O	90	2×10^{-5}	48	2×10^{4}	-	-	-
	H	90	2×10^{-5}	54	2×10^{6}	-	-	-
NIP-3T-Rdb	O	90	1×10^{-4}	47	3×10^{4}	1×10^{-5}	−50	1×10^{2}
	H	90	1×10^{-4}	46	5×10^{3}	5×10^{-6}	−15	3×10^{1}
NIP-3T-Py	H	90	4×10^{-4}	8	2×10^{2}	-	-	-
	O	90	1×10^{-2}	42	9×10^{2}	-	-	-
NIP-3T-TIPS	H	90	-	-	-	4×10^{-5}	−31	2×10^{1}

[a] Electron carrier mobility (μ) is given in $cm^2\ V^{-1}\ s^{-1}$ and threshold voltages (V_T) in V. [b] Device parameters reported are for films grown on hexamethyldisilazane vapor-treated Si/SiO_2 substrates (H) or octadecyltrichlorosilane-treated Si/SiO_2 substrates (O). [c] Deposition temperature.

The implementation of conjugated molecular assemblies into polymeric materials has proven to be an efficient strategy to develop new semiconductors for a wide variety of applications.[19][20][21][22] Among them, the development of metal-free, organic polymers as photocatalysts[23] for the removal of hazardous contaminants[24][25] has been revealed as an emerging area in the last decade.

In this regard, molecular- and polymeric-conjugated assemblies with wide absorption cross-section characteristics are good candidates as photocatalysts. Moreover, it is known that materials which combine electron donor and electron acceptor units are also interesting in photocatalysis because fast recombination processes may be inhibited. The possibilities offered by the oligothiophene–naphthalimide assemblies to efficiently tune their optical and electronic properties as well as their suitability to be functionalized at the α positions of the oligothiophene moieties make these types of assemblies good candidates to be used as monomers for the syntheses of donor-acceptor polymeric materials suitable for the photocatalytic degradation of organic pollutants in water.[26]

Poly(azomethine) network **NIP-3T-ANW** (Figure 6) was prepared under solvothermal reaction conditions.[27] Interestingly, this polymeric material shows high thermal stability, without noticeable weight loss up to 450 °C, in contrast with the **NIP-3T** molecular semiconductor in which the degradation starts at 200 °C. Furthermore, the material exhibits a good energy band alignment for the photodegradation of some organic pollutants, such as rhodamine B (**RhB**). Due to the above characteristics, the potential of **NIP-3T-ANW** as photocatalyst in the photodegradation of **RhB** has been investigated. It is known that RhB is stable in aqueous solution under illumination in the absence of catalyst. In contrast, when **NIP-3T-ANW** is added, after 120 min, almost a 90% of **RhB** is degraded in the aqueous solution, and no stability problems in the catalyst are detected after four catalytic cycles. For comparison purposes, the photocatalytic activity of the analogue molecular component **NIP-3T** has been also investigated, showing only a 55% degradation of RhB in the same time period. Thus, the incorporation of the D-A unit into the polymeric network dramatically increases its activity and allows for its recyclability without losing efficiency (Figure 8).

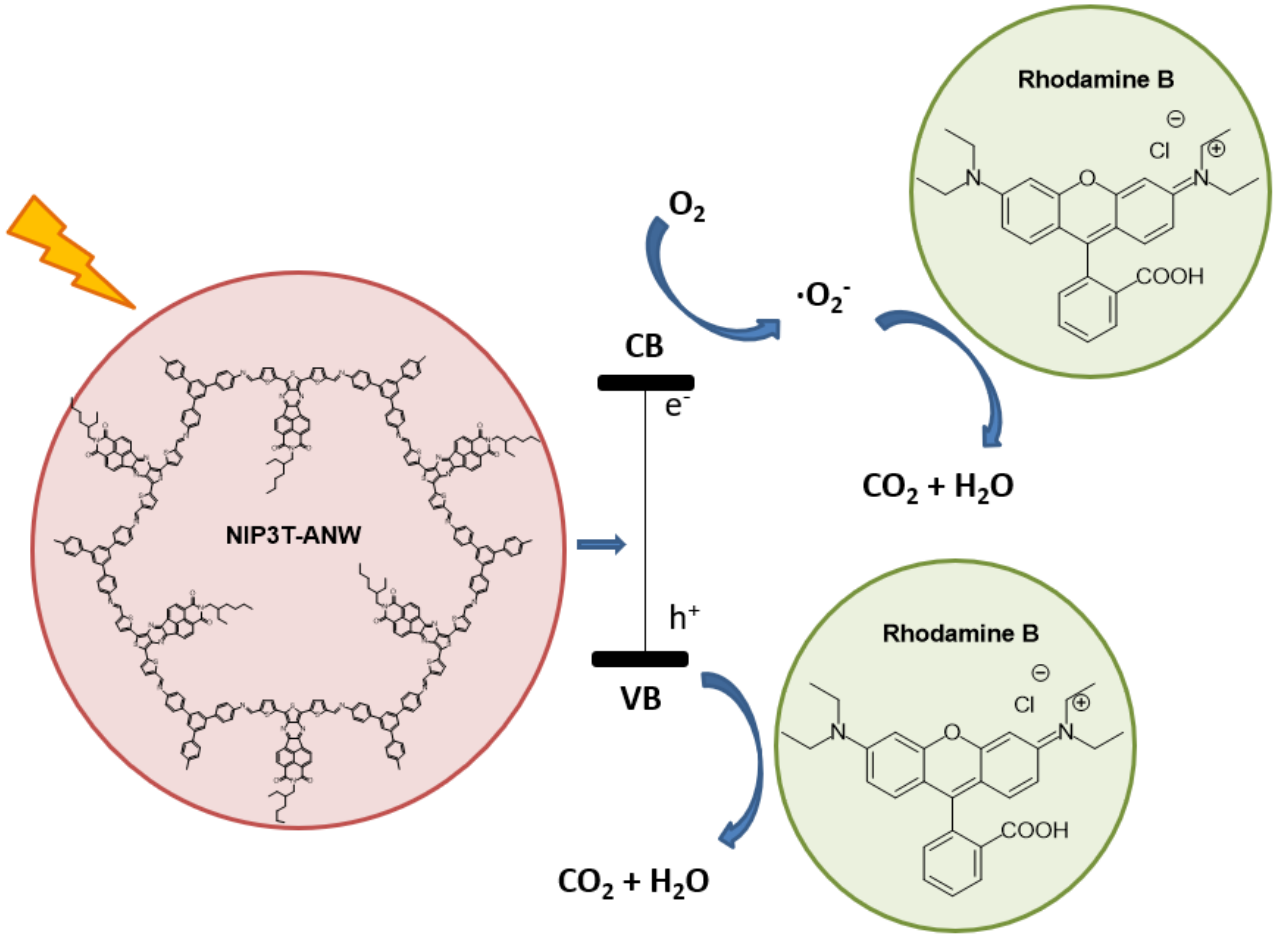

Figure 8. Structure of **NIP-3T-ANW** and its photocatalytical activity

5. Conclusions

In this article, we have described and compared several families of oligothiophene–naphthalimide assemblies synthesized in the group of José L. Segura in which the donor and the acceptor units are connected through different rigid heterocycles. The synthetic modifications in the molecular structure, by growing the oligothiophene or the rylenimide moieties, is translated into a precise control over the frontier molecular orbital energy levels, allowing for the segregation of the HOMO and the LUMO in the molecule, promoting better charge carrier pathways. Studies carried out in the group of Rocío Ponce-Ortiz show that the structural modifications in these molecular systems produce changes in the microstructure domains, in the crystal diffraction patterns and in the electrical performance found in the thin-film organic field-effect transistors. Moreover, it has been shown that the modification of the naphthalimide–oligothiophene central core is not the only effective way to promote order into the molecule. In fact, the introduction of lateral hydrophilic or hydrophobic chains or end-capped terminal groups also represent interesting approaches to obtain organized assemblies via supramolecular interplay, such as Van der Waals interactions or π–π stacking. Finally, the incorporation of these D-A assemblies into polymeric structures produces innovative materials with applications in different fields, including the photocatalytic degradation of organic pollutants in aqueous media.

We believe that the approaches outlined in this feature article concerning the precise modification of frontier molecular orbital energies and topologies in D-A assemblies based on oligothiophene–naphthalimide semiconductors can pave the way in the near future for the design and synthesis of more efficient materials for (opto)electronics and photocatalysis.

References

1. Xugang Guo; Antonio Facchetti; Tobin J. Marks; Imide- and Amide-Functionalized Polymer Semiconductors. *Chemical Reviews* **2014**, *114*, 8943-9021, 10.1021/cr500225d.
2. Huiliang Sun; Lei Wang; Yingfeng Wang; Xugang Guo; Imide-Functionalized Polymer Semiconductors. *Chemistry – A European Journal* **2018**, *25*, 87-105, 10.1002/chem.201803605.

3. Alexandra F. Paterson; Saumya Singh; Kealan Fallon; Thomas Hodsden; Yang Han; Bob C. Schroeder; Hugo Bronstein; Martin Heeney; Iain McCulloch; Thomas D. Anthopoulos; et al. Recent Progress in High-Mobility Organic Transistors: A Reality Check. *Advanced Materials* **2018**, *30*, e1801079, 10.1002/adma.201801079.

4. Jie Yang; Zhiyuan Zhao; Shuai Wang; Yunlong Guo; Yunqi Liu; Insight into High-Performance Conjugated Polymers for Organic Field-Effect Transistors. *Chem* **2018**, *4*, 2748-2785, 10.1016/j.chempr.2018.08.005.

5. Naomi Sakai; Jiri Mareda; Eric Vauthey; Stefan Matile; Core-substituted naphthalenediimides. *Chemical Communications* **2010**, *46*, 4225-4237, 10.1039/c0cc00078g.

6. Naihang Zheng; Zuzhang Lin; Yuanhui Zheng; Dong Li; Jie Yang; Weifeng Zhang; Liping Wang; Gui Yu; Room-temperature stable organic spin valves using solution-processed ambipolar naphthalenediimide-based conjugated polymers. *Organic Electronics* **2020**, *81*, 105684, 10.1016/j.orgel.2020.105684.

7. Jyoti Shukla; Pritam Mukhopadhyay; Synthesis of Functionalized Naphthalene Diimides and their Redox Properties. *European Journal of Organic Chemistry* **2019**, *2019*, 7770-7786, 10.1002/ejoc.201901390.

8. Xiaowei Zhan; Antonio Facchetti; Stephen Barlow; Tobin J. Marks; Mark A. Ratner; Michael R. Wasielewski; Seth R. Marder; Rylene and Related Diimides for Organic Electronics. *Advanced Materials* **2010**, *23*, 268-284, 10.1002/adma.201001402.

9. Xugang Guo; Mark D. Watson; Conjugated Polymers from Naphthalene Bisimide. *Organic Letters* **2008**, *10*, 5333-5336, 10.1021/ol801918y.

10. Rocío Ponce Ortiz; Helena Herrera; Raúl Blanco; Hui Huang; Antonio Facchetti; Tobin J. Marks; Yan Zheng; José L. Segura; Organic n-Channel Field-Effect Transistors Based on Arylenediimide-Thiophene Derivatives. *Journal of the American Chemical Society* **2010**, *132*, 8440-8452, 10.1021/ja1018783.

11. Rocío Ponce Ortiz; Helena Herrera; Carlos Seoane; José L. Segura; Antonio Facchetti; Tobin J. Marks; Rational Design of Ambipolar Organic Semiconductors: Is Core Planarity Central to Ambipolarity in Thiophene-Naphthalene Semiconductors?. *Chemistry – A European Journal* **2011**, *18*, 532-543, 10.1002/chem.201101715.

12. Raúl Blanco; Rafael Gómez; Carlos Seoane; José L. Segura; Elena Mena-Osteritz; Peter Bäuerle; An Ambipolar Peryleneamidine Monoimide-Fused Polythiophene with Narrow Band Gap. *Organic Letters* **2007**, *9*, 2171-2174, 10.1021/ol0706861.

13. Sandra R. González; Juan Casado; Juan Teodomiro López Navarrete; Raúl Blanco; José L. Segura; A β-Naphthaleneimide-Modified Terthiophene Exhibiting Charge Transfer and Polarization Through the Short Molecular Axis. Joint Spectroscopic and Theoretical Study. *The Journal of Physical Chemistry A* **2008**, *112*, 6732-6740, 10.1021/jp802228a.

14. Alejandro De La Peña; Iratxe Arrechea-Marcos; María J. Mancheño; M. Carmen Ruiz Delgado; J. Teodomiro López Navarrete; José L. Segura; Rocío Ponce Ortiz; Tuning of the Electronic Levels of Oligothiophene-Naphthalimide Assemblies by Chemical Modification. *Chemistry – A European Journal* **2016**, *22*, 13643-13652, 10.1002/chem.201602082.

15. A. Riaño Carnerero; G. López Espejo; M. J. Mancheño Real; Brian Eckstein; R. C. González-Cano; F. S. Melkonyan; A. Facchetti; T. J. Marks; J. Casado; J. T. López Navarrete; et al. Even and odd oligothiophene-bridged bis-naphthalimides for n-type and ambipolar organic field effect transistors. *Journal of Materials Chemistry C* **2017**, *5*, 9439-9450, 10.1039/c7tc02023f.

16. Helena Herrera; Paula De Echegaray; Marta Urdanpilleta; Maria J. Mancheño; Elena Mena-Osteritz; Peter Bäuerle; José L. Segura; Linear and star-shaped naphthalimide-fused pyrazinacenes. *Chemical Communications* **2013**, *49*, 713-715, 10.1039/c2cc36791b.

17. Paula De Echegaray; María J. Mancheño; Iratxe Arrechea-Marcos; Rafael Juárez; Guzmán López-Espejo; J. Teodomiro López Navarrete; María Mar Ramos; Carlos Seoane; Rocío Ponce Ortiz; José L. Segura; et al. Synthesis of Perylene Imide Diones as Platforms for the Development of Pyrazine Based Organic Semiconductors. *The Journal of Organic Chemistry* **2016**, *81*, 11256-11267, 10.1021/acs.joc.6b02214.

18. Matías J. Alonso-Navarro; Alexandra Harbuzaru; Paula de Echegaray; Iratxe Arrechea-Marcos; Albert Harillo-Baños; Alejandro de la Peña; María Del Mar Ramos; Juan Teodomiro Lopez Navarrete; Mariano Campoy-Quiles; Rocío Ponce Ortiz; et al. Effective interplay of donor and acceptor groups for tuning optoelectronic properties in oligothiophene–naphthalimide assemblies. *Journal of Materials Chemistry C* **2020**, *8*, 15277-15289, 10.1039/d0tc03026k.

19. Min Wang; Paul Baek; Alireza Akbarinejad; David Barker; Jadranka Travas-Sejdic; Conjugated polymers and composites for stretchable organic electronics. *Journal of Materials Chemistry C* **2019**, *7*, 5534-5552, 10.1039/c9tc00709a.

20. Przemyslaw Ledwon; Daria Ovsiannikova; Tomasz Jarosz; Szymon Gogoc; Pawel Nitschke; Wojciech Domagala; Insight into the properties and redox states of n-dopable conjugated polymers based on naphtalene diimide units. *Electrochimica Acta* **2019**, *307*, 525-535, 10.1016/j.electacta.2019.03.169.

21. Jungho Lee; Eun-Sol Shin; Yeon-Ju Kim; Yong-Young Noh; Changduk Yang; Controlling the ambipolarity of thieno-benzo-isoindigo polymer-based transistors: the balance of face-on and edge-on populations. *Journal of Materials Chemistry C* **2019**, *8*, 296-302, 10.1039/c9tc05641f.
22. Kui Li; Lei Wang; Zhongxin Chen; Xianfeng Yang; Yu-Xiang Yu; Wei-De Zhang; Ye Wang; Yumeng Shi; Kian Ping Loh; Qing-Hua Xu; et al. Photocatalytic Hydrogen Evolution under Ambient Conditions on Polymeric Carbon Nitride/Donor-π-Acceptor Organic Molecule Heterostructures. *Advanced Functional Materials* **2020**, *30*, 2005106, 10.1002/adfm.202005106.
23. Guigang Zhang; Zhi-An Lan; Xinchen Wang; Conjugated Polymers: Catalysts for Photocatalytic Hydrogen Evolution. *Angewandte Chemie International Edition* **2016**, *55*, 15712-15727, 10.1002/anie.201607375.
24. Fangyuan Chen; Weijia An; Li Liu; Yinghua Liang; Wenquan Cui; Highly efficient removal of bisphenol A by a three-dimensional graphene hydrogel-AgBr@rGO exhibiting adsorption/photocatalysis synergy. *Applied Catalysis B: Environmental* **2017**, *217*, 65-80, 10.1016/j.apcatb.2017.05.078.
25. Ziyang Deng; Jianhua Zhou; Lei Miao; Chengyan Liu; Ying Peng; Lixian Sun; Sakae Tanemura; The emergence of solar thermal utilization: solar-driven steam generation. *Journal of Materials Chemistry A* **2017**, *5*, 7691-7709, 10.1039/c7ta01361b.
26. Matías J. Alonso-Navarro; Jesús Barrio; Sergio Royuela; Neeta Karjule; M. Mar Ramos; José Ignacio Martínez; Menny Shalom; José L. Segura; Photocatalytic degradation of organic pollutants through conjugated poly(azomethine) networks based on terthiophene–naphthalimide assemblies. *RSC Advances* **2021**, *11*, 2701-2705, 10.1039/d0ra10379a.
27. José L. Segura; María J. Mancheño; Félix Zamora; Covalent organic frameworks based on Schiff-base chemistry: synthesis, properties and potential applications. *Chemical Society Reviews* **2016**, *45*, 5635-5671, 10.1039/c5cs00878f.
